



Enhancement in power factor due to anti-correlation between electrical conductivity and thermoelectric power and induced magnetic ordering in high mobility Zn doped Bi₂Te₃ topological insulator



Abhishek Singh ^a, P. Shahi ^b, A.K. Ghosh ^c, J.G. Cheng ^{b,d}, Sandip Chatterjee ^{a,*}

^a Department of Physics, Indian Institute of Technology (Banaras Hindu University), Varanasi, 221005, India

^b Beijing National Laboratory for Condensed Matter Physics and Institute of Physics, Chinese Academy of Sciences, Beijing, 100190, China

^c Department of Physics, Banaras Hindu University, Varanasi, 221005, India

^d School of Physical Sciences, University of Chinese Academy of Sciences, Beijing, 100190, China

ARTICLE INFO

Article history:

Received 5 July 2017

Received in revised form

5 October 2017

Accepted 6 October 2017

Available online 7 October 2017

Keywords:

Topological insulator

Magneto-transport properties

Thermoelectric power factor

ABSTRACT

Electrical resistivity, thermoelectric power, magnetotransport and magnetization of Zn doped Bi₂Te₃ Topological Insulator were studied. Electrical conductivity is enhanced at higher Zn concentration, and the carrier mobility estimated from Hall data reaches a remarkable value of $\sim 7200 \text{ cm}^2 \text{ V}^{-1} \text{ s}^{-1}$. Large positive magnetoresistance (MR $\sim 400\%$) is observed in high mobility samples. Interestingly it is found that the coupling between electrical conductivity and Seebeck coefficient is broken for higher Zn doped Bi₂Te₃ samples which effectively enhances the thermoelectric power factor (from 2.1 mW/K²m for Bi₂Te₃ to 4.64 mW/K²m for Zn doped Bi₂Te₃).

© 2017 Elsevier B.V. All rights reserved.

1. Introduction

Topological insulators (TIs) are a new class of materials characterized by an insulating bulk but conducting at the surface which are topologically protected by time reversal symmetry due to the locking of spin and orbital states [1], and because of this the delocalized surface state (SS) are unaffected from nonmagnetic dopants and defects. The exotic properties in TIs such as possibility of Majorana Fermions, novel magnetoelectric quantum states, topological superconductivity, the absence of backscattering from nonmagnetic impurities, exciton condensation, magnetic monopole and anomalous quantum Hall effect [1–9] in TIs are very promising in the application of quantum computing and spintronic devices. Quantum magneto-transport phenomenon such as weak antilocalization [10–12], Aharonov-Bohm oscillations [13], and quantum conductance fluctuations [14], are associated with topological surface states and it was confirmed using Angle-resolved

photoemission spectroscopy (ARPES) in Bi₂Te₃ and Bi₂Se₃TIs [15,16].

Moreover large Thermoelectric power in these materials are very important as Thermoelectric (TE) devices are considered a promising means of energy saving and power generation. These devices use two types of materials viz. *n* type and *p* type, connected in series. The efficiency of a TE materials can be evaluated by the dimensionless figure of merit, $ZT = \{(\sigma s^2)T/\kappa\}$ where σ , s , T and κ respectively are the electrical conductivity, Seebeck coefficient, temperature and thermal conductivity of the materials. Significant efforts have been made for increasing the thermoelectric figure of merit in different materials, including silicides [17], half-Heuslers [18,19], and tellurides (e.g. of Bi [20], Pb [21,22] and Ge [23]). By increasing the power factor (PF) = σs^2 or decreasing the thermal conductivity we can improve the performance of a TE devices. Mobility of carrier and different scattering mechanisms control the transport properties. Carrier mobility is strongly influenced by the magnetic field, which in turn affects the transport properties including resistivity [24–26]. As a matter of fact, Magnetoresistance (MR) of a TE material gives valuable information regarding the mechanism affecting conductivity, and therefore is intimately

* Corresponding author.

E-mail address: schatterji.app@itbhu.ac.in (S. Chatterjee).

related to the underlying physics towards obtaining materials with high ZT values. Furthermore, the materials having magnetoresistive response can open a new way for the dispersion and dynamics of the charge carriers which can be exploited for the technical use such as multifunctional electromagnetic applications, mechatronics and disc reading heads [27]. Zero band gap materials exhibit fascinating and superior electronic properties compared to non-zero band gap materials [28]. In zero band gap materials the energy required to make a transition from valence band to conduction band can be arbitrarily low which leads to finite electrical conductivity under an infinitesimal perturbation. Moreover electrical transport properties such as resistance or conductance are very sensitive to external effect such as pressure, electrical and magnetic fields, is a unique feature in zero band gap materials. Abrikosov [29] has proposed a quantum model for the materials having zero-gap and linear dispersion. According to this model, magnetoresistance (MR) for the zero gap materials should be giant, linear and temperature independent which is ideal for practical applications. Besides these, based on two dimensional random register network Parish and Littlewood has given a classical model for the explanation of MR in the inhomogeneous system having strong disorder such as $\text{Ag}_{2\pm\delta}\text{Se}$ and $\text{Ag}_{2\pm\delta}\text{Te}$, nonmagnetic graphene and InSb system [30–32].

When the TIs are doped by the magnetic element, weak localization (WL) effect is seen and as a result time reversal symmetry (TRS) breaking and surface state band gap opening could be realized [33–35]. Therefore, for the protection of TRS we have doped nonmagnetic Zn in Bi_2Te_3 topological insulator. Here we report that Zn doping in Bi_2Te_3 TI increases the power factor (by enhancing simultaneously electrical conductivity and thermopower) along with the mobility and magnetoresistance, and this decoupling of electrical conductivity and thermopower is the more effective way to enhance the thermoelectric power factor. The materials having such type of promising properties may be very useful for the application point of view such as in refrigeration, quantum computing, multifunctional electromagnetic applications, mechatronics and disc reading heads.

2. Experimental details

The single crystals of $\text{Bi}_{2-x}\text{Zn}_x\text{Te}_3$ ($x = 0, 0.10, 0.20$) were prepared by using modified Bridgman method [36]. High purity powder of Bi (99.999%), Te (99.999%) and Zn (99.999%) were mixed uniformly in their stoichiometric ratios. The mixture was sealed in quartz tube after evacuating down to $\sim 10^{-6}$ torr. The crystal growth involves cooling from 950°C to 550°C in 24 h and annealing at this temperature for 72 h. Thus obtained silver colored single crystals were then cooled down to room temperature slowly. For phase identification X-ray powder diffraction (XRD) measurements were carried out with $\text{Cu K}\alpha$ radiation using a Rigaku (MiniFlex II DEX-TOP) powder diffractometer (the cleaved surface is shiny and ~ 5 mm in size). Hall effect and magneto-transport measurements were performed on single crystals by standard four probe technique. These measurements were carried out as a function of magnetic field and temperature by using Quantum Design Physical Property Measurement system (PPMS). Magnetic properties have been performed by using Quantum Design Magnetic property measurement system (MPMS SQUID).

3. Results and discussion

In order to characterize the obtained single crystals, we have shown X-ray diffraction (XRD) patterns at room temperature in Fig. 1. All diffractions peaks are exclusively labeled with (00L) i.e. (003), (006), (0015), (0018) and (0021) indices, all indexed peak

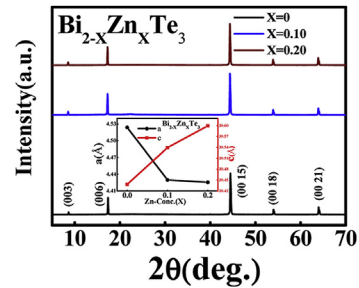


Fig. 1. Room temperature X-ray diffraction patterns of $\text{Bi}_{2-x}\text{Zn}_x\text{Te}_3$ ($x = 0, 0.10, 0.20$) single crystals, Inset: Variation of lattice parameter with Zn concentration for $\text{Bi}_{2-x}\text{Zn}_x\text{Te}_3$ ($x = 0, 0.10, 0.20$).

matches with JCPDS card no-15-0863 with space group R-3m, indicating that the samples are single crystalline and the cleaved surface is the basal plane perpendicular to the c axis without any secondary phases and impurity. An additional peak around $2\theta = 40^\circ$ for the samples is observed which might be due to the slight misalignment or slight tilt angle of the crystallinity of as cleaved single crystals. Around $2\theta = 54^\circ$ and 64° , a small splitting due to the difference in the wavelength of X-ray source of $\text{CuK}\alpha_1$ and $\text{CuK}\alpha_2$ radiation is observed.

The lattice parameter $a = b$ obtained from the XRD analysis for the Hexagonal setting is 4.52 \AA for $x = 0$, and it slightly decreases with increasing Zn concentration and finally going to 4.42 \AA for $x = 0.20$ (shown in Inset of Fig. 1), because the ionic radius of Zn is smaller than that of Bi. The obtained lattice parameter value well matched with the reported value [36]. In addition, the peak position shifts to lower angle in Zn-doped Bi_2Te_3 which might be due to the increase in c parameter from 30.43 \AA (for $x = 0$) to 30.59 \AA (for $x = 0.20$) as shown in inset of Fig. 1. The slightly elongated c parameter in doped sample cannot however compensate the decreased a or b parameter in maintaining same lattice volume, leading to smaller cell volume. The change in lattice parameter gives clear evidence that Zn is sufficiently substituted for Bi in Bi_2Te_3 .

The resistivity behaviour from 2 K to 300 K under zero magnetic field for $\text{Bi}_{2-x}\text{Zn}_x\text{Te}_3$ ($x = 0, 0.10, 0.20$) are displayed in Fig. 2. Resistivity of doped samples first increases at $x = 0.10$, and then it decreases for $x = 0.20$. The presence of impurity (Zn) in the host material Bi_2Te_3 may be a reason of increasing resistivity in doped sample up to $x = 0.10$. But at the higher concentration at $x = 0.20$, resistivity decreases which might be due to the increase in mobility which will be discussed below.

Magnetization (M) as a function of magnetic field (H) of the Zn

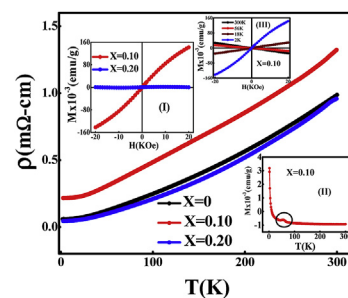


Fig. 2. Temperature dependence of zero field electrical resistivity for $\text{Bi}_{2-x}\text{Zn}_x\text{Te}_3$ samples ($X = 0, 0.10, 0.20$) and Inset I is showing the field dependence of magnetization (MH) for $\text{Bi}_{2-x}\text{Zn}_x\text{Te}_3$ ($X = 0.10$ and 0.20) samples, Inset II is showing magnetization Vs temperature (MT) curve for $X = 0.10$ sample and Inset III is showing MH curve for $X = 0.10$ sample at different temperatures viz. 2 K, 18 K, 56 K, 300 K.

doped $\text{Bi}_{2-x}\text{Zn}_x\text{Te}_3$ ($x = 0.10, 0.20$) single crystals was measured at 2 K in the H range -2 T to 2 T in the inset I of Fig. 2. It is obvious from the M(H) curve that all the Zn doped Bi_2Te_3 samples show ferromagnetism. It is also observed from M(H) curve that magnetization increases with increase of Zn content to $x = 0.10$ but the value of magnetization decreases for $x = 0.20$ (shown in inset I of Fig. 2). Local magnetization of Zn atom may be the reason of induced ferromagnetism in our doped samples. We have also shown magnetization as a function of temperature for $x = 0.10$ (sample with highest magnetization value in the present investigation) in the Inset II of Fig. 2. The anomaly around 55 K may be an indication of local magnetization due to Zn atoms. The M(H) behaviour of $x = 0.1$ at different temperatures are shown in inset III Fig. 2 which shows the evolution of ferromagnetism with temperature.

The variation of thermopower (S) with temperature of the as-grown single crystals of $\text{Bi}_{2-x}\text{Zn}_x\text{Te}_3$ ($x = 0, 0.10, 0.20$) are also shown in inset of Fig. 3 in the temperature range of 2 K-300 K. The sign of the thermopower is found to be negative, which suggests that the majority of carriers are electrons. The maximum absolute value of S obtained in the case of pure Bi_2Te_3 is $142.8 \mu\text{V/K}$ at 300 K, consistent with values reported by Cao et al. [37]. The S value initially increases with doping Zn and with further doping of Zn the value of S remains constant. This might be due to the fact that S is additive in nature. The S attains the maximum value at $227.9 \mu\text{V/K}$ for $x = 0.20$. To determine the efficiency of thermoelectric power we have calculated the power factor (PF) using the formula

$$\text{Power Factor} = \sigma S^2$$

where σ is the electrical conductivity and S is the thermopower. Variation of PF with temperature for the $\text{Bi}_{2-x}\text{Zn}_x\text{Te}_3$ ($x = 0, 0.10, 0.20$) single crystals is shown in Fig. 3. It is observed that with the increase in temperature electrical resistivity increases in pure and $x = 0.10$ doped samples but the increase in S is much larger than the increase of electrical resistivity which gives rise to the increase of power factor with increasing temperature for the $x = 0.10$ sample. In $x = 0.20$ sample further increment in PF is observed. In fact, the convenient route to enhance the PF for TE materials is the use of dopants [38,39]. A lot of work has been done for the enhancement of thermopower and the power factor in Bi_2Te_3 [40–43]. The reported value of the PF by Na et al. in Bi_2Te_3 thin film was $1.47 \times 10^{-3} \text{ W/K}^2\text{m}$ [40], whereas Shang have found the value as $7.08 \times 10^{-4} \text{ W/K}^2\text{m}$ for the sputtered Bi_2Te_3 thin film [41]. The PF achieved by Bottner et al. was $1.57 \times 10^{-3} \text{ W/K}^2\text{m}$ for *n*-type Bi_2Te_3 materials [42]. The PF value reported by Han et al. was below $2.4 \times 10^{-3} \text{ W/K}^2\text{m}$ at room temperature in $\text{Bi}_2\text{Te}_{3-x}\text{Se}_x$ alloys [43]. Jiang et al. have found that it was $2.7 \times 10^{-4} \text{ W/K}^2\text{m}$ and $2.2 \times 10^{-4} \text{ W/K}^2\text{m}$ in *p*-type and *n*-type $\text{ZnO/Bi}_2\text{Te}_3$ composite, respectively, at room temperature [44]. In our case the obtained value of PF is much larger than those reported, which will be discussed below.

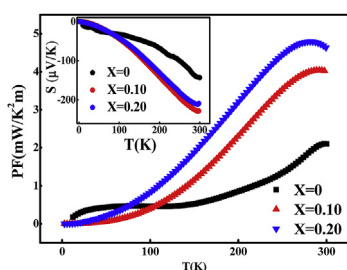


Fig. 3. Variation of power factor (PF) as a function of temperature for $\text{Bi}_{2-x}\text{Zn}_x\text{Te}_3$. Inset: represents the thermopower of the $\text{Bi}_{2-x}\text{Zn}_x\text{Te}_3$.

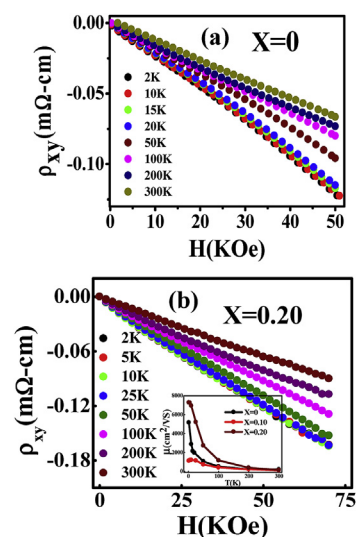


Fig. 4. (a) Magnetic field dependence of the Hall resistivity at different temperatures for Bi_2Te_3 . (b) Magnetic field dependence of the Hall resistivity at different temperatures for $x = 0.20$ sample. Inset: Variation of mobility as a function of temperature for $\text{Bi}_{2-x}\text{Zn}_x\text{Te}_3$ ($x = 0, 0.10, 0.20$).

In order to confirm the carrier type and to determine its mobility and concentration we have performed Hall measurement on the pure and doped samples. Fig. 4(a) and (b) show the variation of Hall resistivity as a function of applied magnetic field at different temperatures for $x = 0$ and 0.20 samples respectively. Both samples show a negative slope of Hall effect indicating *n* type carrier for the entire range of doping and temperature of measurement, which is also consistent with the negative S of the pure and Zn doped samples. We have determined the carrier concentration at different temperatures from the Hall data using the formula $N = 1/R_H e$, where R_H is the Hall coefficient and e is the charge of electron. As the temperature increases N value increases, which should be attributed to the increased bulk contribution. But the estimated carrier concentration remains almost constant ($\sim 10^{19}$) upon doping which is consistent with the reported value [45,46]. The carrier mobility (μ) has been evaluated using the relation $\mu = \frac{1}{\rho N e}$, where ρ is the electrical resistivity of the samples. It is clear from the inset of Fig. 4 (b) that mobility decreases with increasing temperature as in a typical metal. At low temperatures, the mobility first decreases for $x = 0.1$ and then increases substantially for $x = 0.2$ which is obvious from inset of Fig. 4(b).

Variation of magnetoresistance as a function of applied magnetic field under different temperatures are shown in Fig. 5. Magnetoresistance (MR) of the samples has been defined as, $\text{MR}\% = \frac{R(H) - R(0)}{R(0)} \times 100\%$ where $R(H)$ is the resistance at applied magnetic field H, $R(0)$ is the measured resistance at $H = 0$. MR for all the samples increases with applied field but decreases with increasing temperature. A clear linear and non-saturating MR can be seen for the entire range of temperature and field of measurement for all of the samples as shown in Fig. 5. A clear dip could be seen in the doped samples $x = 0.10, 0.20$ [shown in inset of Fig. 5(d)] which is not present in case of pure sample $x = 0$. Moreover, the observed maximum MR reaches $\sim 400\%$ for $x = 0.10$ sample and is almost 16% higher than the parent ($x = 0$) sample.

It is obvious from the MR graph that it is completely symmetric for all the undoped and doped samples with respect to the reversal of the magnetic field direction, ruling out any possible contribution from Hall voltage. Moreover, it is obvious from the MR curve that for the low doped sample ($x = 0.1$), it is completely linear without

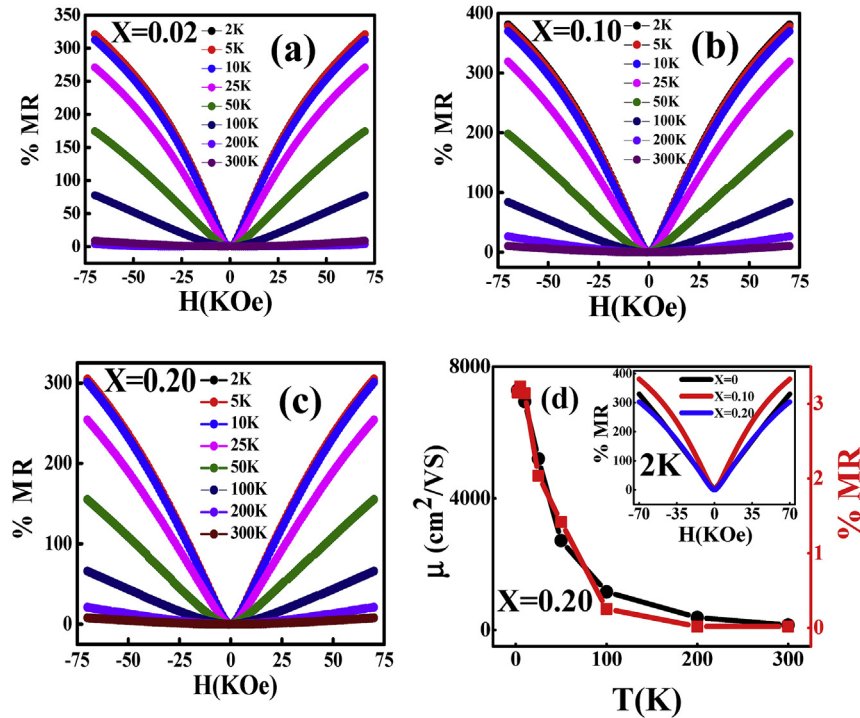


Fig. 5. (a, b, c). Normalized MR as a function of magnetic field at different temperatures $\text{Bi}_{2-x}\text{Zn}_x\text{Te}_3$ ($x = 0, 0.10, 0.20$). (d) Variation of mobility and MR as a function of temperature for the sample $x = 0.20$ at low field. Inset: Variation of MR at 2 K for $\text{Bi}_{2-x}\text{Zn}_x\text{Te}_3$ ($x = 0, 0.10, 0.20$).

any sign of saturation except at the very low field where a dip in MR is observed which might be due to the existence of weak anti-localization (WAL) that results from the surface state. As the Zn content increases the MR dip is broadened indicating reduction of the surface state [shown in inset of Fig. 5(d)]. As we increase temperature, MR becomes linear for intermediate temperature range and again at higher temperature i.e. 300 K it is showing quadratic behaviour. Similar type of quadratic growth behaviour without any sign of saturation has been seen at high temperature in Bi_2Te_3 films by Wang et al. [47]. As is mentioned above, the sharp resistance dip at $T = 2$ K is an indication of the presence of a weak anti-localization (WAL) effect [48] and as we increase temperature, MR dip broadened at low field because at higher T phase coherence length decreases [11].

To understand the origin of observed MR we have considered the theoretical models viz. quantum model by Abrikosov [29] and classical model by Parish and Littlewood [30]. According to the quantum model [29], when extreme quantum limit $\hbar\omega_c > E_F$ is satisfied, all the electrons are condensed into one Landau level where $\hbar\omega_c$ is the cyclotron energy and E_F is the Fermi energy. But later experimental studies indicate that LMR could appear even at smaller field when electron occupy several Landau levels [32]. We have estimated the crossover field using the inequality

$$n_0 \ll \left(\frac{eH}{\hbar c}\right)^{3/2}$$

considering the carrier density of the order of $10^{19}/\text{cm}^3$ from Hall measurement, the estimated crossover field was larger than 10 T where n_0 is the carrier concentration, e is the electron charge, H is the strength of applied field and c is the speed of light. But in our case we have crossover field less than 3 T (estimated from dMR/dH). Moreover, according to generic quantum description of galvano-magnetic phenomenon, the longitudinal MR can be represented as $\rho_{xx} = \rho_{yy} = \frac{N_i H}{\pi N^2 e c}$, where ρ_{xx} and ρ_{yy} are the transverse component of magnetoresistance, N_i is the concentration of static scattering centers, N is the density of electrons.

According to this formula resistance is inversely related to the square of the carrier concentration which is also not well matched with our experimental data. Moreover, this quantum MR should be linear down to very small fields and should be non saturating and positive and more importantly it should be temperature independent but in our case MR is temperature independent up to 10 K only and for the higher temperatures MR is strongly temperature dependent and therefore we conclude that Abrikosov quantum model may not be applicable here.

According to the classical model [49], magnitude of the fluctuations in mobility is an important factor for the origin of MR. Furthermore, in classical case it is expected that the value of crossover field shifts with the temperature, as fluctuations in mobility would dominate at higher temperatures. It is observed in Fig. 5(d) that both mobility and MR decrease with increase of temperature and the nature of variations are similar. This behaviour is consistent with the PL model [49], hence we expect that the better explanation may be close to classical case.

From the above discussion it is clear that Zn doping enhances the bulk contribution and the bulk contribution playing the significant role in MR and also to increase the mobility. Moreover, it is very interesting that while moving from $x = 0.1$ to $x = 0.2$ both σ and S increase which is very unusual. In fact, in most of the cases, as S decreases σ increases and vice-versa. The simultaneous enhancement of σ and S is observed in $x = 0.2$ sample indicating that S is dominated by bulk. It is observed that up to $x = 0.1$ the coupling between σ and S persists. But with further increase of doping concentration σ and S is decoupled. For both the cases PF increases. For the former case the enhancement of S is more effective than the decrease in σ . On the other hand, in the latter case both σ and S increase which enhance the PF significantly. In fact, the thermopower and the electrical conductivity are both intimately related with the carrier concentration and mobility. In the present investigation, it is observed that the mobility increases

significantly for highest Zn doped sample [inset of Fig. 4(b)]. In general, in conventional semiconductors, the carrier mobility is lowered by induced defects. These defects which are produced by doping are the scattering centers. Moreover, it has already been reported that in addition to the bulk transport, Bi₂Te₃ exhibits significant surface transport, which is attributed to the topological insulating state [45]. In the present case the defects (created with Zn doping) cause the unusual mobility behaviour by modifying the relative contribution of conduction electrons between the bulk and the surface. With Zn doping the bulk state is enhanced in expense to the surface state than in the undoped sample where surface conduction weighs more as is clear from the MR and Hall data. Therefore, although μ initially decreases with Zn doping, the μ shows an increase with further doping [as shown in inset of Fig. 4(b)], because with doping the higher-mobility bulk conduction plays a much more significant role than the surface conduction.

The simultaneous enhancement of S and σ is observed only in relatively high doped samples, which suggests that the thermopower is dominated by the bulk contribution that can be tailored by the defects. In the relaxation time model, the thermopower in the degenerate doping limit is given by:

$$S = \frac{K}{e} \left(\frac{\pi^2 KT}{3\epsilon_F} \right) \left(\frac{3}{2} + r \right)$$

where r is the index of the electron relaxation time related to kinetic energy [50] and ϵ_F , the Fermi energy is measured from the conduction band edge. The above equation not only predicts the ordinary decrease of S as n increases (through ϵ_F), but also an increase in S when r increases. The former leads to the conventional inverse coupling between S and σ , while the latter allows the decoupling of them, as seen in the present case. In fact, r varies from $-1/2$ for acoustic phonon scattering to $3/2$ for ionized impurity scattering [50]. Initially for the undoped and low doped samples, the measured S follows the trend with calculation using $r = -1/2$, indicating that electrons are mostly scattered by phonons in these samples. This is consistent with theoretical prediction that electrical transport in Bi₂Te₃ at similar carrier concentrations ($\approx 1 \times 10^{19} \text{ cm}^{-3}$) is limited by phonon scattering [51]. However, the high doping causes a transition of the scattering mechanism from phonon-dominated ($r = -1/2$) to impurity-dominated ($r = 3/2$); as a result, the thermopower is drastically enhanced. This transition is also confirmed by the fact that the mobility μ of undoped sample increases rapidly at low temperatures, while μ is less temperature-sensitive for doped sample. The defect induced decoupling of S and σ naturally leads to a significant increase in the thermoelectric power factor, $S^2\sigma$, as shown in Fig. 3. It reaches a peak value of $4.64 \times 10^{-3} \text{ W/K}^2\text{m}$ for $x = 0.20$ which is two times larger than that of the undoped Bi₂Te₃ ($2.1 \times 10^{-3} \text{ W/K}^2\text{m}$). The value of PF reported in the present investigation in Zn doped Bi₂Te₃ TI system is the largest to the best of our knowledge. Moreover, it is expected that the thermal conductivity will also be reduced for the highly doped samples. Therefore, a significant improvement of the thermoelectric performance can be achieved through a proper doping. Similar behaviour is observed by inducing native defects in topological insulator [52].

4. Conclusions

Electrical resistivity, magnetotransport and thermoelectric properties of Bi_{2-x}Zn_xTe₃ single crystals were studied. Magnetoresistance shows the linear field dependence and with Zn content the MR value increases. The MR behaviour above 10 K cannot be explained with quantum model, but is consistent with the classical model. The mobility initially decreases with Zn doping but with

further doping mobility increases indicating increasing contribution of bulk in expense of surface state. For the $x = 0.2$ sample, the electrical conductivity and thermopower are simultaneously enhanced, leading to a significant enhancement of thermoelectric power factor.

Acknowledgement

The authors are grateful to CIFC, IIT(BHU) for providing facility for magnetic measurement.

References

- [1] M.Z. Hasan, C.L. Kane, Rev. Mod. Phys. 82 (2010) 3045–3067.
- [2] L. Fu, C.L. Kane, Phys. Rev. Lett. 102 (2009) 216403.
- [3] L.A. Wray, S.-Y. Xu, Y. Xia, Y.S. Hor, D. Qian, A. V.Fedorov, H. Lin, A. Bansil, R.J. Cava, M.Z. Hasan, Nat. Phys. 6 (2010) 855–859.
- [4] Y.S. Hor, A.J. Williams, J.G. Checkelsky, P. Roushan, J. Seo, Q. Xu, H.W. Zandbergen, A. Yazdani, N.P. Ong, R.J. Cava, Phys. Rev. Lett. 104 (2010) 057001.
- [5] X.L. Qi, S.C. Zhang, Rev. Mod. Phys. 83 (2011) 1057–1110.
- [6] P. Roushan, J. Seo, C.V. Parker, Y.S. Hor, D. Hsieh, D. Qian, A. Richardella, M.Z. Hasan, R.J. Cava, A. Yazdani, Nature (London) 460 (2009) 1106–1110.
- [7] B. Seradjeh, J.E. Moore, M. Franz, Phys. Rev. Lett. 103 (2009) 066402.
- [8] X.-L. Qi, R. Li, J. Zhang, S.-C. Zhang, Science 323 (2009) 1184–1187.
- [9] R. Yu, W. Zhang, H.-J. Zhang, S.-C. Zhang, X. Dai, Z. Fang, Science 329 (2010) 61–64.
- [10] J.G. Checkelsky, Y.S. Hor, R.J. Cava, N.P. Ong, Phys. Rev. Lett. 106 (2011) 196801.
- [11] H.T. He, G. Wang, T. Zhang, I.K. Sou, G.K.L. Wong, J.N. Wang, H.Z. Lu, S.Q. Shen, F.C. Zhang, Phys. Rev. Lett. 106 (2011) 166805.
- [12] J. Chen, H.J. Qin, F. Yang, J. Liu, T. Guan, F.M. Qu, G.H. Zhang, J.R. Shi, X.C. Xie, C.L. Yang, K.H. Wu, Y.Q. Li, L. Lu, Phys. Rev. Lett. 105 (2010) 176602.
- [13] H.L. Peng, K.J. Lai, D.S. Kong, S. Meister, Y.L. Chen, X.L. Qi, S.C. Zhang, Z.X. Shen, Y. Cui, Nat. Mater. 9 (2010) 225–229.
- [14] J.G. Checkelsky, Y.S. Hor, M.-H. Liu, D.-X. Qu, R.J. Cava, N.P. Ong, Phys. Rev. Lett. 103 (2009) 246601.
- [15] Y.L. Chen, J.G. Analytis, J.-H. Chu, Z.K. Liu, S.-K. Mo, X.L. Qi, H.J. Zhang, D.H. Lu, X. Dai, Z. Fang, S.C. Zhang, I.R. Fisher, Z. Hussain, Z.X. Shen, Science 325 (2009) 178–181.
- [16] Y. Xia, D. Qian, D. Hsieh, L. Wray, A. Pal, H. Lin, A. Bansil, D. Grauer, Y.S. Hor, R.J. Cava, M.Z. Hasan, Nat. Phys. 5 (2009) 398–402.
- [17] Y. Gelbstein, J. Tunbridge, R. Dixon, M.J. Reece, H.P. Ning, R. Gilchrist, R. Summers, I. Agote, M.A. Lagos, K. Simpson, C. Rouaud, P. Feulner, S. Rivera, R. Torrecillas, M. Husband, J. Crossley, I. Robinson, J. Electron. Mater. 43 (2014) 1703–1711.
- [18] O. Appel, M. Schwall, M. Kohne, B. Balke, Y. Gelbstein, J. Electron. Mater. 42 (2013) 1340–1345.
- [19] O. Appel, T. Zilber, S. Kalabukhov, O. Beeri, Y. Gelbstein, J. Mater. Chem. C 3 (2015) 11653–11659.
- [20] Roi Vizeal, Tal Bargig, Ofer Beeri, Yaniv Gelbstein, J. Electron. Mater. 45 (2016) 1296–1300.
- [21] Yaniv Gelbstein, J. Electron. Mater. 40 (2011) 533–536.
- [22] Yaniv Gelbstein, Acta Mater. 61 (2013) 1499–1507.
- [23] Boaz Dado, Yaniv Gelbstein, Dimitri Mogilansky, Vladimir Ezersky, Moshe P. Daril, J. Electron. Mater. 39 (2010) 2165–2171.
- [24] A. Banerjee, B. Fauque, K. Izawa, A. Miyake, I. Sheikin, J. Flouquet, B. Lenoir, K. Behnia, Phys. Rev. B 78 (2008), 161103(R).
- [25] G.J. Snyder, E.S. Toberer, Nat. Mater. 7 (2008) 105–114.
- [26] S.X. Zhang, R.D. McDonald, A. Shekhter, Z.X. Bi, Y. Li, Q.X. Jia, S.T. Picraux, Appl. Phys. Lett. 101 (2012) 202403.
- [27] Xiaolin Wang, Yi Du, Shixue Dou, Chao Zhang, Phys. Rev. Lett. 108 (2012) 266806.
- [28] X.L. Wang, Phys. Rev. Lett. 100 (2008) 156404.
- [29] A.A. Abrikosov, Phys. Rev. B 58 (1998) 2788–2794.
- [30] A.L. Friedman, J.L. Tedesco, P.M. Campbell, J.C. Culbertson, E. Aifer, F.K. Perkins, R.L. Myers-Ward, J.K. Hite, C.R. Eddy, G.G. Jernigan, D.K. Gaskill, Nano Lett. 10 (2010) 3962–3965.
- [31] R. Xu, A. Husmann, T.F. Rosenbaum, M.-L. Saboungi, J.E. Enderby, P.B. Littlewood, Nature (London) 390 (1997) 57–60.
- [32] J.S. Hu, T.F. Rosenbaum, Nat. Mater. 7 (2008) 697–700.
- [33] Hai-Zhou Lu, Junren Shi, Shun-Qing Shen, Phys. Rev. Lett. 107 (2011) 076801.
- [34] Minhao Liu, Jinsong Zhang, Cui-Zu Chang, Zuoqiang Zhang, Xiao Feng, Kang Li, Ke He, Li-li Wang, Xi Chen, Xi Dai, Zhong Fang, Qi-Kun Xue, Xucun Ma, Yayu Wang, Phys. Rev. Lett. 108 (2012) 036805.
- [35] Judy J. Cha, Martin Claassen, Desheng Kong, Seung SaeHong, Kristie J. Koski, Xiao-Liang Qi, Yi Cui, Nano Lett. 12 (2012) 4355–4359.
- [36] Y.S. Hor, P. Roushan, H. Beidenkopf, J. Seo, D. Qu, J.G. Checkelsky, L.A. Wray, D. Hsieh, Y. Xia, S.-Y. Xu, D. Qian, M.Z. Hasan, N.P. Ong, A. Yazdani, R.J. Cava, Phys. Rev. B 81 (2010) 195203.
- [37] H. Cao, R. Venkatasubramanian, C. Liu, J. Pierce, H. Yang, M.Z. Hasan, Y. Wu,

- Y.P. Chen, Appl. Phys. Lett. 101 (2012) 162104.
- [38] J.R. Sootsman, D.Y. Chung, M.G. Kanatzidis, Angew. Chem. Int. Ed. 48 (2009) 8616–8639.
- [39] W.S. Liu, Q.Y. Zhang, Y.C. Lan, S. Chen, X. Yan, Q. Zhang, H. Wang, D.Z. Wang, G. Chen, Z.F. Ren, Adv. Energy Mater. 1 (2011) 577–587.
- [40] Jongbeom Na, Younghoon Kim, Teahoon Park, Chihyun Park, Eunyoung Kim, ACS Appl. Mater. Interfaces 8 (2016) 32392–32399.
- [41] H. Shang, H. Gu, Y. Zhong, F. Ding, G. Li, F. Qu, H. Zhang, Z. Dong, H. Zhang, W. Zhou, J. Alloys Compd. 690 (2017) 851–855.
- [42] H. Böttner, J. Nurnus, A. Gavrikov, G. Kühner, M. Jäggle, C. Künzel, D. Eberhard, G. Plescher, A. Schubert, K.-H. Schlereth, J. Microelectromech. Syst. 13 (2004) 414–420.
- [43] S.T. Han, P. Rimal, C.H. Lee, H.-S. Kim, Y. Sohn, S.-J. Hong, Intermetallics 78 (2016) 42–49.
- [44] Q. Jiang, J. Yang, J. Xin, Z. Zhou, D. Zhang, H. Yan, J. Alloys Compd. 694 (2017) 864–868.
- [45] H. Li, Y.R. Song, Meng-Yu Yao, Fang Yang, Lin Miao, Fengfeng Zhu, Canhua Liu, C.L. Gao, Dong Qian, X. Yao, Jin-Feng Jia, Y.J. Shi, D. Wu, Appl. Phys. Lett. 101 (2012) 072406.
- [46] Y.H. Choi, N.H. Jo, K.J. Lee, J.B. Yoon, C.Y. You, M.H. Jung, J. Appl. Phys. 109 (2011), 07E312.
- [47] Z.H. Wang, L. Yang, X.J. Li, X.T. Zhao, H.L. Wang, Z.D. Zhang, Xaun P.A. Gao, Nano Lett. 14 (2014) 6510–6514.
- [48] S. Hikami, A.I. Larkin, Y. Nagaoka, Prog. Theor. Phys. 63 (1980) 707–710.
- [49] M.M. Parish, P.B. Littlewood, Phys. Rev. B 72 (2005) 094417.
- [50] F.D. Rosi, Solid State Electron. 11 (1968) 833–868.
- [51] Bao-Ling Huang, Massoud Kaviani, Phys. Rev. B 77 (2008) 125209.
- [52] J. Suh, K.M. Yu, D. Fu, X. Liu, F. Yang, J. Fan, D.J. Smith, Y.-H. Zhang, J.K. Furdyna, C. Dames, W. Walukiewicz, J. Wu, Adv. Mater. 27 (2015) 3681–3686.